Real-time, non-invasive analysis of biocatalytic PET degradation

*Ronny Frank, Dana Krinke, Christian Sonnendecker, Wolfgang Zimmermann, Heinz-Georg Jahnke**

Dr. R. Frank, Dr. Dana Krinke, Dr. H.G. Jahnke
Centre for Biotechnology and Biomedicine, Molecular biological-biochemical Processing Technology, Leipzig University
Deutscher Platz 5, D-04103 Leipzig, Germany
Email: heinz-georg.jahnke@bbz.uni-leipzig.de

Dr. C. Sonnendecker, Prof. Dr. W. Zimmermann
Institute of Analytical Chemistry, Leipzig University
Johannisallee 29, D-04103 Leipzig, Germany

Keywords: Electrochemical impedance spectroscopy, free-standing polymer film, polyester biodegradation, 3D printing, screening platform, PHL7, LCC

Abstract

The Earth has entered the *Anthropocene*, branded by ubiquitous and devastating environmental pollution from plastics such as polyethylene terephthalate (PET). Sustainable and at the same time economical solutions for recycling are more urgently sought than ever. With the recovery of the starting materials, the selective biodegradation of PET by polyester hydrolases is an appealing solution. To accelerate the search for high-performance biocatalysts, we demonstrate how changing dielectric properties of PET films can be used to evaluate potent polyester hydrolases. For this purpose, the PET film separates two reaction chambers in an impedimetric setup to quantify the film thickness-dependent change in capacitance. There is no need for any pretreatment or nano particle production, commonly associated with PET analysis. The derived reaction rates line up very well with comparative methods such as weight loss, VSI, and HPLC measurements. The developed monitoring system enables both high temporal resolution and high parallelizability. Compared to

optical methods, this technique is also insensitive to changes in solution composition. It is therefore particularly suitable as a screening method for any PET films, enzyme libraries and additives. Furthermore, using AFM images and FEM simulations, we show how the technique can be extended to a perforation analysis.

1. Introduction

Polymer chemistry is one of the most advanced branches of material science that has produced synthetics that are indispensable in industry, medicine, research, and everyday life. These plastics often have physical, chemical and physiological properties that are designed for an optimal performance and often do not offer options for an end-of life recycling. Thus, the replacement with more sustainable plastic solutions is often associated with usability drawbacks, higher costs or unavailability on a larger production scale. The largest amount of the produced plastic is used in the packaging industry (40 %).[1] Most plastics are not biodegradable and the raw material for their synthesis is primarily petroleum-based. In view of the crises of global warming and pollution in the *Anthropocene*, the environmentally compatible and sustainable transformation of polymer chemistry represents a major challenge. So-called bioplastics, which are bio-based materials, however not necessarily biodegradable or vice versa,[2] still remain a niche market accounting for only 1% of the global plastic production.[3] Apart from the expenditure to establish bioplastic production on an industrial level, materials such as polylactide [4], thermoplastic starch,[5] or polyhydroxyalkanoates [6] rarely fulfil the mechanical and physicochemical requirements (stability, moisture barrier, heat deformation temperature, hydrophobicity) for an extended

spectrum of applications unless used in blends. They also suffer from a low processability and their production is still too cost-intensive compared with petrochemical-based plastics.[3]

A part of polymer chemistry's transformation can be achieved by tertiary recycling, thereby closing the loop from plastic synthesis back to its reuse, especially if the starting materials of the polymers are recovered in an efficient and sustainable way.[7] PET accounts for 10% of the total plastic production world-wide which reached 359 million tons in 2018.[1] PET is widely used in the packaging and beverage industries and for the manufacture of textiles.[8]

Besides energy-intensive tertiary chemical recycling by hydrolysis, glycolysis or pyrolysis,[9] recycling of polyesters such as polyethylene terephthalate (PET) with enzymes has attracted attention. Several polyester hydrolases, especially cutinase-like enzymes derived from bacterial or fungal origin show high PET-degrading activity.[10] Thermostable PET hydrolases efficiently degrade PET with a high amorphous content but not crystalline or the biaxial-oriented (BO) PET of beverage bottles.[11] Cutinases degrade the natural polyester cutin in the cuticle of plant cells, and are produced by pathogenic and saprophytic fungi and bacteria. A rather unspecific substrate recognition allows those enzymes also to attack synthetic polyesters such as PET or polycaprolactone.[12] The products released by the enzymatic cleavage of PET are terephthalate (TPA), mono(2-hydroxyethyl terephthalate) (MHET), *bis*(2-hydroxyethyl terephthalate) (BHET) and ethylene glycol (EG).[10b, 13] The enzymatic polymer hydrolysis occurs more rapidly near the glass transition temperature of PET at around 70°C. Therefore, thermostability of the biocatalysts is a prerequisite for an efficient depolymerisation.[14] The search for high-performance polyester hydrolases is tedious because few high-throughput or high-content screening systems exist to detect PET-degrading activity.[15] In contrast, most analytical techniques such as NMR, SEM, HPLC and calorimetry are

used for the detailed investigation of PET degradation, but are not suitable for high-throughput screening purposes.[16]

Here we developed a non-invasive, contact-free tool to monitor the enzymatic degradation of PET films by real-time electrochemical impedance spectroscopy. This approach offers a straightforward way to reach a high degree of parallelisation by established multiplexing techniques, compared to typical methods such as gravimetry or the pH-stat. This tool is also not prone to interferences from additives, thereby representing an alternative to optical methods. We show that electrochemical impedance spectroscopy is suitable for the fast screening of biocatalytic activities and the elucidation of the enzymatic polymer degradation mechanism. A major advantage is that the degradation of PET can be studied directly without the need for using model compounds,[17] or the prior generation of nano particles.[18] Any type of PET material can thereby be examined independent of its manufacturing process. This opens up the possibility of detecting novel PET hydrolases that can also decompose biaxially oriented PET or PET of higher crystallinity. In addition to obtaining enzyme kinetic data, high-speed impedance measurements also allow to analyze the enzymatic degradation process during pore formation in PET films in detail. Thus, this tool has the potential for high-throughput as well as high-content screening applications for plastic-degrading enzymes, not only for PET but also for thin plastic films in general.

2. Results and Discussion

2.1. Impedance measurement setup

The determination of the degradation of PET films was based on high-precision impedance spectroscopy. For this purpose, we developed a two-chamber reaction vessel (Figure 1A) with

a PET film as the thinnest material barrier between the two chambers filled with electrolyte and determined the impedance between the chambers. To the best of our knowledge this is the first report on such a setup. The few studies that used impedance spectroscopy to analyze degradation effects always used non-conductive polymers or coatings directly on an electrode material.[19] This was often accompanied by delamination effects that compromised the validity of the impedimetric analysis.[20] With the setup of a free-standing polymer film, this issue is precluded. The first chamber was provided by means of a 3D-printed insert made of polypropylene, which was mounted with the PET film. The PET reaction window was defined on the inside by the geometry of the insert (Figure S1) and on the outside by an epoxy resin coating to prohibit enzymatic PET degradation outside the reaction window. The inserts were placed in a standard 2 mL reaction tube as the 2nd chamber. A lid with two platinum electrodes formed a two-electrode setup for impedance spectroscopy with one electrode on each side of the PET film. The platinum electrodes were chosen as large as possible to minimize self-impedance. The reaction vessel was placed in a standard thermoblock to achieve the optimal temperature required for the enzymatic reaction and to prevent external temperature changes that would influence the impedance measurements. In this sealed system, the impedance was recorded over a wide frequency range from 50 Hz to 5 MHz using a high-precision impedance analyzer and a multiplexer to observe multiple reaction units simultaneously (Figure 1B). PET degradation was observed over a period of several hours to days, while a single measurement could be performed within seconds. Thus, multiplexing was ideal for screening purposes, because a high temporal resolution for 96 or more reaction units could be achieved with a single impedance analyzer. During the enzymatic degradation of the PET film, its thickness decreased (Figure 1C), which had a direct influence on the impedance signal. The PET film acted as a capacitive resistor determining the impedance signal until pores

formed in the PET film allowing an ion flow between the chambers (Figure 1D). From this point on, there was a multi-decadal decrease in the magnitude of the impedance within seconds, due to the size, length and localization of the pores, which now determined the total impedance as an ohmic resistance. By determination of the changes in impedance recorded from the starting time of the enzymatic reaction to just before the pore formation event, kinetics of the bulk PET film degradation could be derived. The raw impedance data were analyzed using the simplified *Randles* equivalent circuit model.[20-21] While the capacitance C and ohmic resistance R2 in parallel could be related to the PET film, there was an additional ohmic resistance R1, coming from the multiplexer, the contact and platinum wires and the bulk electrolyte, which summed up to 90 Ω when measured with a reaction vessel without a PET film (Figure S2). Thus, R1 was kept constant during the equivalent circuit modelling procedure.

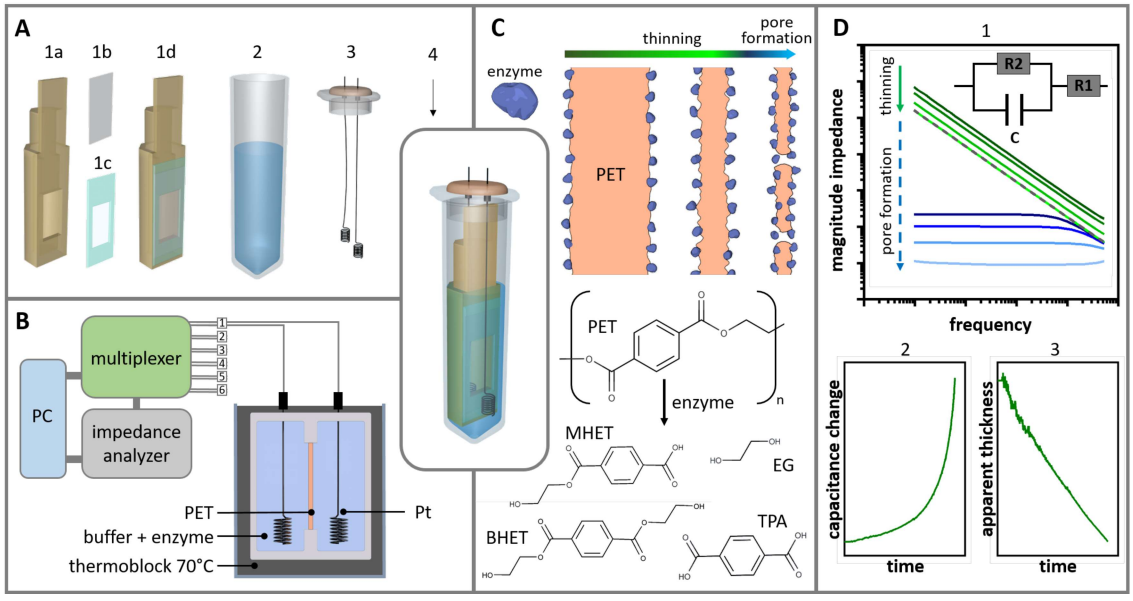

Figure 1: Impedance-based measurement setup for enzymatic G-PET film degradation analysis. A Assembly of a two-chamber reaction vessel. The 3D-printed polypropylene unit (1a) is combined with a PET film (1b) to define a reaction window with epoxy resin (1c),

finished insert (1d); 2) 2 mL reaction vessel, 3) lid with platinum electrodes, 4) complete reaction unit. **B** Components of the impedance measurement system. **C** Illustration of the enzymatic degradation of a G-PET film, leading to the products mono(2-hydroxyethyl)-terephthalic acid (MHET), *bis*(2-hydroxyethyl)-terephthalic acid (BHET), terephthalic acid (TPA) and ethylene glycol (EG). **D** Impedance raw data derived from a degradation experiment (1) were analyzed by a *Randles* equivalent circuit model to give the change in capacitance (2) and from this in turn the apparent PET film thickness (3). Additional graphs can be found in Figure S6.

To relate the capacitance C to the PET film, first we considered the capacitance $C_{t=0}$ according to equation 1, which is the sum of the capacitance of the PET film (C_{PET}) and a capacitance of the rest of the system (C_{rest}). The geometry of the PET film was a planar rectangle, with an electrode on each of its sides. C_{PET} depends on the area (A) of the film, its relative permittivity (ε_r) and the film thickness (d), according to equation 2. Although the platinum electrodes themselves were not rectangular, the electrolyte of the reaction solution covered the PET film from both sides, acting due to its high conductivity similar to common electrolytic capacitors where this equation applies. A change in the total capacitance during an enzymatic degradation experiment was caused by a change in the PET film thickness (d), while there was almost no change in capacitance without enzyme as could be shown in control experiments (Figure S3). Thus, C_{rest} could be assumed to be constant, leading to equation 3. By combining equation 3 with equation 1 we derived equation 4, which was free of C_{rest}. C_{rest} was determined to be about 10 pF (Figure S4). Solving equation 4 for the thickness expression, resulted in equation 5 representing the time-dependent apparent change of the PET film thickness. The initial thickness of the PET film ($d_{PET,t=0}$) was derived from a mechanical measurement at room

temperature), and corresponded for a 225 µm film thickness to a capacitance of 4.6 pF using the manufacturer's specification of the relative permittivity (ε_r = 3.0). Since the enzymatic degradation of the PET was performed at 70°C, a correction for the thermal expansion was considered, which for a thermal expansion coefficient of 2-8·10^{-5} K^{-1} according to the manufacturer's specification gave a maximal deviation of just +0.81 µm for the 225 µm film, and thus could be neglected. In contrast, the temperature-dependence of ε_r is far more important. The capacitance of the initial PET film at 70°C as derived from approximation experiments using different sized reaction windows led to a value of 5.1 pF that would fit to a 225 µm film thickness assuming an ε_r of 3.3. This is in line with the extent of temperature-dependence of ε_r observed for PET [22] and correlated well with a FEM simulation (Figure S5). Thus, we calculated all thickness values with an ε_r of 3.3 for the measurement frequency range.

$$C_{t=0} = C_{PET,t=0} + C_{rest} \quad (1)$$

$$C_{PET,t=0} = \frac{\varepsilon_0 \varepsilon_r A}{d_{PET,t=0}} \quad (2)$$

$$C_{t=0} + \Delta C = \frac{\varepsilon_0 \varepsilon_r A}{d_{PET,t=0} + \Delta d_{PET}} + C_{rest} \quad (3)$$

$$C_{PET,t=0} + \Delta C = \frac{\varepsilon_0 \varepsilon_r A}{d_{PET,t=0} + \Delta d_{PET}} \quad (4)$$

$$d(t) = d_{PET,t=0} + \Delta d_{PET}(t) = \frac{\varepsilon_0 \varepsilon_r A}{C_{PET,t=0} + \Delta C(t)} \quad (5)$$

2.2. Correlation of PET film thickness derived from impedance and optical data

In the next step, we correlated the thickness data derived from impedance measurements to data we extracted from optical analysis of the PET film surface in phase contrast-imaging as well as start- and endpoint mechanical measurements (Figure 2). For this, we modified the

design of the polypropylene insert to equip it with a glass plate of 1 mm thickness on the backside to allow light microscopic analysis (Figure 2B). During the degradation of the PET sample, craters were forming on both sides of the film. Adjacent craters formed edges ideal for optical focussing (Figure 2C) with a precision of ±1 µm. These structures were verified by scanning electron and atomic force microscopy (AFM). The thickness of the PET film was calculated as described by McLaren et al. [23] using a refractive index of 1.61 for the PET fim (according to the manufacturer's specification) and an optical power P of zero, given the planar character of the PET film. Figure 2A shows that the mechanical and optical measurements fitted well together, while the impedance data showed a more pronounced decrease in the apparent film thickness over time. The mechanical and the optical measurements probably slightly overestimated the mean thickness of the PET film, due to the edges of the craters which were in contact or in focus during the measurement, and thus did not include the mean decrease in thickness according to the depth of the craters. We estimated this effect to contribute possibly up to 3 µm for each side of the PET film, resulting in a total of 6 µm as deviation based on the AFM data. However, this effect was obviously insufficient to explain the difference we observed in the impedance data of up to 30 µm. The most straightforward explanation we connected to the change in surface roughness effecting the PET film capacitance. In this case, with increasing roughness, the surface area increased enabling more charge to be stored. The inverse relation between capacitance and film thickness would then lead to an apparent stronger decrease in film thickness. We measured the increase in surface area by AFM (Figure 2D) for image sections of 2 x 2 μm^2 and 60 x 60 μm^2. Within the first hours, we observed the largest change of the surface increase factor starting from almost perfect planarity with 1.00 ± 0.00 (60 µm, 0 h) and 1.00 ± 0.00 (2 µm, 0 h) to reach 1.03 ± 0.00 (60 µm, 2.5 h) and 1.11 ± 0.01 (2 µm, 2.5 h). Within the next 7.5 h the

nanoscopic features (2 x 2 μm^2 images) stayed almost constant at a surface increase factor of 1.10, while the microscopic increase factor (60 x 60 μm^2) diminishes slightly to 1.01. Thus, the nanoscopic roughness attributed by far more to the overall surface area increase than the microscopic one. To investigate the influence of the surface roughness on the capacitance and thus the apparent film thickness, we performed FEM simulations with different surface increase factors (Figure S7). An increase in area of just 5 % led to a capacitance increase by a factor of 1.28, 10 % to an increase by a factor of 1.38, and 15 % to an increase by a factor of 1.44. Thus, the observed surface increase in the range of 10 % was sufficient to explain the difference between the optically/mechanically determined film thickness of 80 µm after 10 h which is equivalent to a film capacitance of 15 pF, and the calculated apparent film thickness of 55 µm based on impedimetric monitoring (equivalent to 20 pF, factor of 1.33). Since the impedimetrically derived film thicknesses can be well understood in this way, the technique is particularly suitable for the characterization of PET films in correlation with high-resolution and topological imaging techniques. Moreover, it is certainly an excellent screening parameter for the evaluation of PET-degrading enzyme activities. We anticipate that by impedance measurements it is possible to detect PET-degrading activity in a wide range of polyester hydrolases due to the expected similarity of their catalytic mechanism.

From a morphological point of view, on the microscopic scale craters were formed which grew with time, while new craters were continuously forming at every stage. The nanoscopic features showed randomly distributed grains of similar size after degradation times from 2.5 h to 10 h. However, notably after 2.5 h, we observed local areas with a lower roughness and a finer graining compared to later stages, which occured particularly in valley regions (see also Figure S8). The finer graining was primarily visible in phase images. We hypothesize that these represent highly disordered amorphous areas, which could be slightly faster degraded than

the coarse-grained areas. After 5 h of degradation, only a few of these amorphous areas could be observed which were spatially very limited, and after a degradation time of 7.5 h they disappeared. We assume that this observed heterogeneity is caused by the thermal treatment in the manufacturing process. In this regard, impedance spectroscopy offers a new approach to study enzymatic PET degradation because of the inherit recording of the surface roughness and moreover, its ability for a high temporal resolution. This allows to profile different types of PET films, which differ in their construction, amorphous and crystalline heterogeneity, and degradability. As an example, we degraded R-PET from a post-consumer PET thermoform clamshell packing (crystallinity 4.5 % [24]), showing a considerable different time-profile compared with the more homogenous virgin G-PET film of similar crystallinity, indicated by zones of faster and slower degradation rates (Figure S9).

Impedimetric monitoring could be combined with detailed topological data and extracted metrics [25] in combination with simulation models to derive a mechanistic insight in the relationship between PET structure and its enzymatic degradation. This requires the collection of additional data, e.g. from AFM, VSI or SEM, which would be appropriate for an in-depth study of enzymatic PET degradation, but is clearly not required for a high-throughput enzyme screening system.

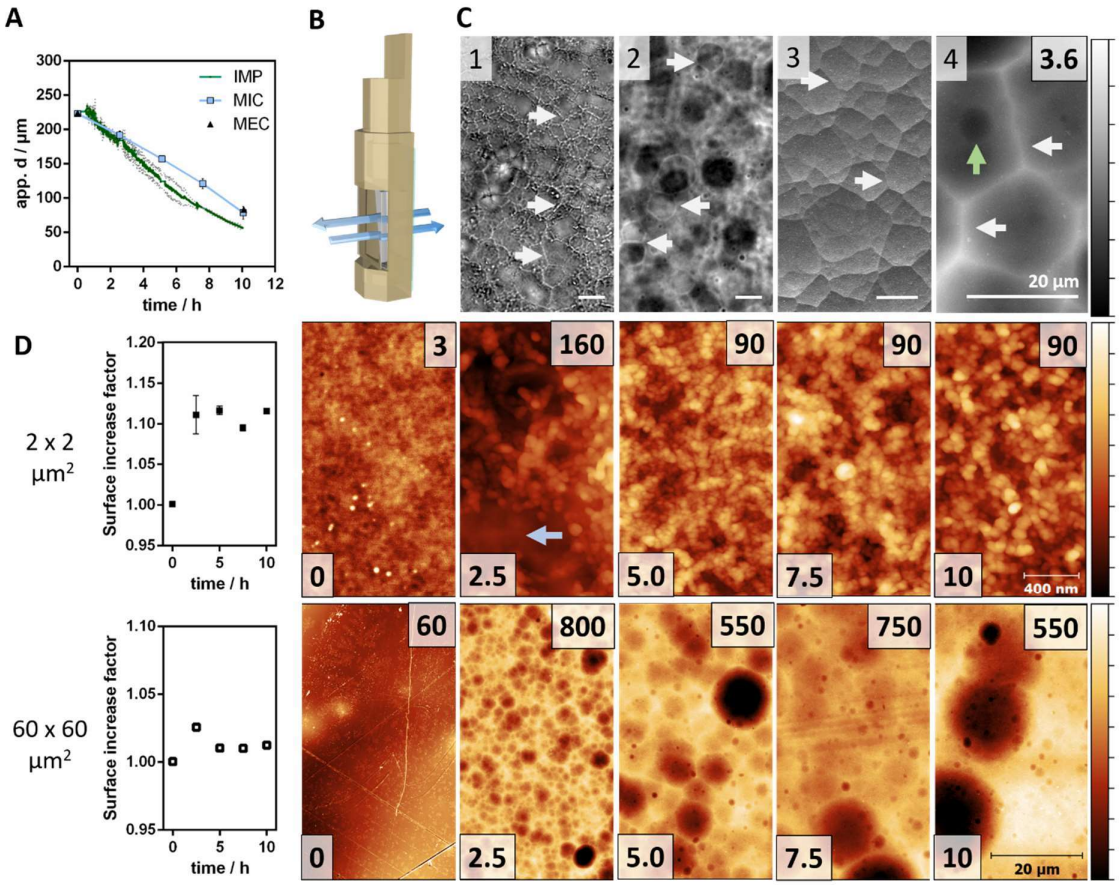

Figure 2: Microscopic analysis of G-PET film thickness and surface roughness. A Thickness data measured impedimetrically (IMP), optically (MIC) and mechanically (MEC) at the same inserts (n=2). **B** 3D-printed polypropylene insert with a glass backside to allow light microscopic imaging. **B** Phase-contrast images of the outside of the PET film (**C1**) and of the inside (**C2**). SEM (**C3**) and AFM (**C4**) image of a PET surface after partial degradation by the polyester hydrolase PHL7 [24] showing crater-like structures. Height scale of AFM image is given as 0 to 3.6 µm. White arrows mark crater edges used for focussing the outside and inside of the PET film. Green arrow marks a fresh degradation zone. **D** Time dependent surface analysis of PET film degradation by PHL7 using AFM in intermittent-contact mode. Height scale is given in nm from zero to value in upper right corner of each image. Time is given as h in the lower

left corner. Blue arrow marks area of low roughness. Surface increase factor extracted from 2 x 2 μm^2 and from 60 x 60 μm^2 512 x 512 px images (mean ± sd, n ≥ 2).

2.3. Enzymatic PET degradation kinetics

Figure 3A shows the apparent rate of G-PET film degradation as a function of enzyme concentration of the highly active polyester hydrolase PHL7. We observed a typical saturation curve, with a V_{max} of -22.5 $\mu m \cdot h^{-1}$ according to a one-site specific binding non-linear regression. The saturation was due to the finite amount of free binding sites on the PET surface. In addition to the analysis of the capacitive change, which enables a real-time quantification of the degradation, the recording of the pore formations in the film furthermore allowed an independent qualitative rate estimation of the enzymatic degradation (Figure 3A2). Here, the multidecadal jump was recorded, which, similar to a yes/no decision, provided information about at what time the film has locally become so thin that ion passage could take place. Since this is also a stochastic process that can occur at different times depending on possible defects in the film, it can only be used as a benchmark for an enzyme evaluation when a sufficiently large number of replicates are available. However, for PET with a high homogenous film thickness and only small or no defects, pore forming events between replicates can also occur temporally quite close to one another, deviating by only one minute after a 13 h reaction time (Figure S10). A major advantage of the high-precision and high-resolution impedance spectroscopy-based monitoring was the ability to analyze the different degradation effects using the same data set.

To demonstrate the suitability of the method for an evaluation of PET-degrading enzyme performance, we determined the degradation rate of the two polyester hydrolases PHL7 and

LCC (Figure 3B).[26] We observed for the applied enzyme concentration of 13.9 µg·mL^{-1} (corresponding to 0.52 $mg_{enzyme}·g_{PET}^{-1}$), a 3.3 ± 0.7 times higher degradation rate for PHL7 (13.45 ± 2.2 µm·h^{-1}) compared with LCC (4.0 ± 2.1 µm·h^{-1}). This ratio is in accordance with previous determinations by vertical scanning interferometry (4.0), weight loss (2.9 ± 0.1) and HPLC (released amount TPA, 4.6 ± 0.5) measurements.[24]

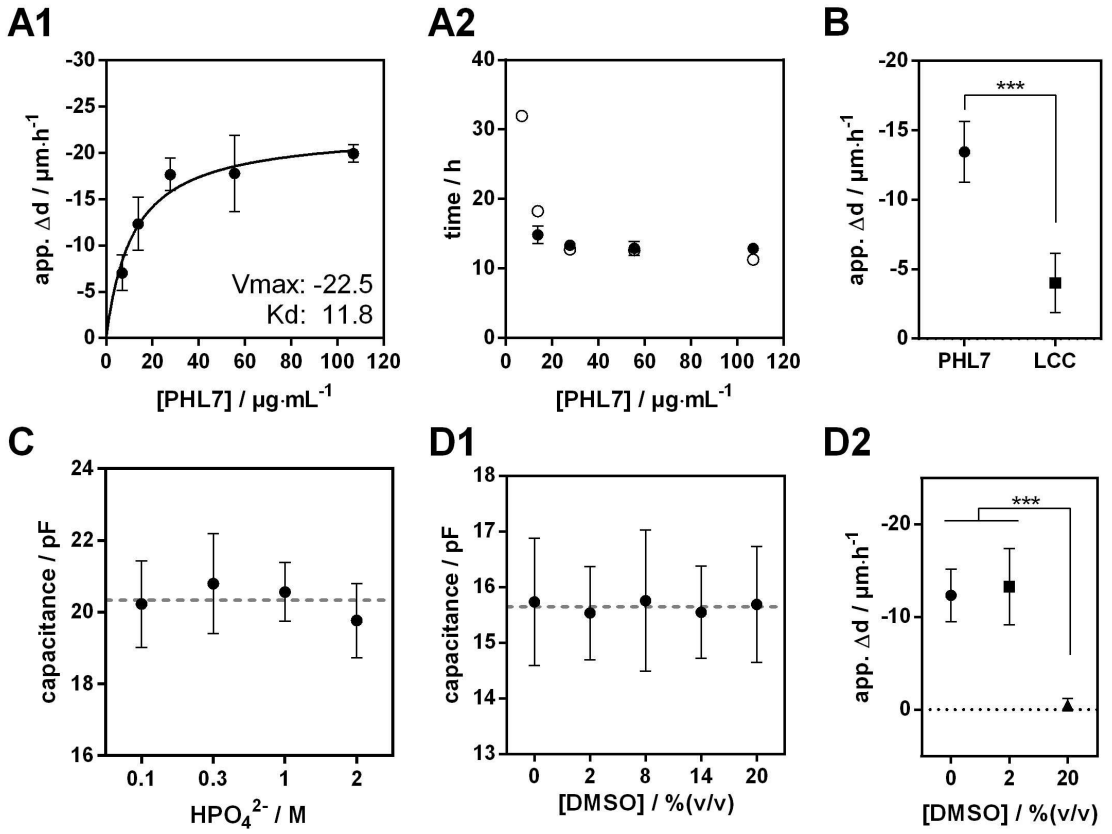

Figure 3: Impedimetrically determined enzymatic degradation of a G-PET film. A1 Saturation curve of PHL7 determined by capacitance assessment. **A2** Time to pore formation of the 225 µm PET film. Closed circles: measured values, open circles: calculated time based on constant initial degradation rate as shown in A1). For the lowest enzyme concentration (6.95 µg·mL^{-1}) no pore formation was observed. **B** Comparison of degradation rates obtained with 0.52 $mg_{enzyme}·g_{PET}^{-1}$ PHL7 and LCC. **C** Influence of hydrogen phosphate buffer

concentration on base capacitance. **D1** Influence of DMSO content on base capacitance. **D2** Activity of PHL7 in the presence of different amounts of DMSO (mean ± sd, n ≥ 3).

We also tested the influence of the electrolyte concentration on the overall capacitance. We found for a range from 0.1 M to 2 M hydrogen phosphate buffer no significant change of the base capacitance (Figure 3C). This is in line with a FEM simulation of thick (225 µm) and thin (12 µm) PET films, where the conductivity of the buffer showed no effect on the impedance spectra (Figure S11). Therefore, the electrolyte concentration could be changed during an experiment without influencing the impedance measurement. This is also crucial since the degradation of PET produces terephthalic acid, thus altering the electrolyte concentration during a reaction. As the impedance measurement only requires a conductive media to derive well-defined spectra, also any other electrolyte should be well suited. We also investigated the effect of different amounts of DMSO, up to 20 % (v/v), on base capacitance and enzyme activity. We chose DMSO as a test solvent, due to its dissolution qualities in the chemical glycolysis of PET to EG and BHET,[27] its good miscibility with water and its low volatility. In the control experiment we observed no significant change in the base capacitance even when 20 % DMSO was present (Figure 3D1). This is especially beneficial for screenings with additives as it demonstrates, that the measurement is not susceptible to a certain degree of non-conducting compounds. Adding DMSO to 2 % did also not alter the degradation rate of PHL7, but inactivated the enzyme at a content of 20 %. This was also confirmed visually, as no dissolution of the PET film was observed. PHL7 inactivation is in accordance with the typical loss in function of enzymes at high organic solvent concentrations.[28]

2.4. Analysis of pore formation in G-PET films degraded with PHL7 by high-speed impedance spectroscopy

During pore formation, when the PET film becomes permeable for ions, the ohmic resistor R2 drops by multiple decades, thus completely altering the impedance signal. In order to measure this event in more detail, a high temporal resolution is required. The lower the excitation frequency, the earlier the pore formation event can be detected, since in this case the ions have more time to create a measurable ion flow even through very small permeation sites. However, low frequencies are accompanied by a longer runtime of the measurement to guarantee sufficient precision. Using a high-precision impedance analyzer optimized for measurement speed especially in the low frequency range, we were able to record impedance spectra of up to six parallel reactions every 1.7 s using a steady multiplexing loop without idle time of the impedance analyzer (Figure 4A). At the breakthrough of the film, the resistance of most of the reaction samples dropped from above 10 MΩ to values between 1-10 KΩ within one minute, before slowly decreasing steadily. In the following minutes, a stepwise stronger decrease in resistance was observed in some cases, probably due to the formation of further pores. We assume that the pore formation started in the crater regions of the film caused by the enzyme when two distinct craters on either side of the PET film happened to be opposite to each other (Figure 4B). When new degradation zones appeared inside the crater, as can be seen in Figure 2C4, a pore could be formed. Due to the crater geometry, the pore would enlarge rapidly due to PET degradation that can now occur not only out-of-plane but also in-plane. To investigate this pore formation process in more detail, we created a FEM model based on a double cone-shaped pore geometry (Figure 4C). Assuming a residual film thickness of 12 µm based on the determined capacitance directly before the first pore formation, we reconstructed the ohmic pore resistance of a high-speed data set (black graph in Figure 4A) to derive the corresponding change in the pore area (Figure S12). Furthermore, the occurrence of a second pore after 17 s was included in the FEM simulation. This model was able to

describe the changes in the impedance spectra most straightforwardly. The combination of impedance spectroscopy and FEM simulation thus allows insight into the enzymatic degradation of PET not only up to the point of pore formation but also beyond. Since impedance spectroscopy is able to monitor the formation of pores in the PET film with a high temporal resolution, it offers in principle another way to determine enzymatic degradation rates. To perform this analysis to gather actual degradation rates, a defined pore would have to be introduced into the PET film, for example by a UV-based femtosecond laser ablation. Due to the high sensitivity of the impedance signal to ion fluxes, this approach could offer a tremendously decreased analysis time from hours or days to minutes. Moreover, due to the minuscule dimension of the required pore, this could be combined with a miniaturisation of the polymer film window resulting in a substantial increase in sample density.

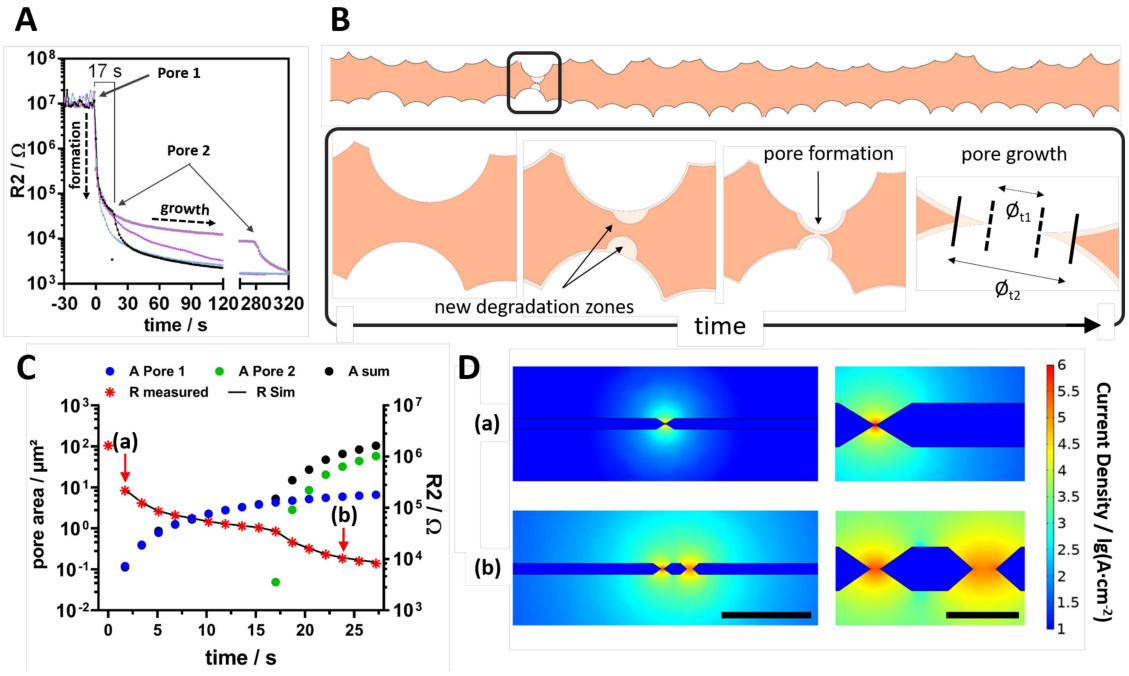

Figure 4: Analysis of pore formation in G-PET film by high-speed impedance spectroscopy. A Ohmic pore resistance as a function of time. Second strong decrease in R2 occurred in one of

the test samples 17 s after the first pore formation, probably indicating the formation of a second pore. **B** Model of the pore formation process. **C** FEM Simulation of the pore formation for the black graph in **A** with a second pore occurring after 17 s. The R2 values derived from the simulated pore area were adjusted to the values for R2 derived from measurements. **D** FEM simulated current density plots for a double cone-shaped pore geometry for time (a) and (b) as marked in C. Scale bar is 50 µm in left images and 10 µm in right images. More plots can be found in the SI (Figure S13).

In conclusion, impedance spectroscopy offers a versatile approach to study the enzymatic degradation of polymer films on multiple mechanistic levels and time scales. The method is robust against changes in electrolyte concentration and works also with a certain content of non-conducting solvents. Analyses can be performed highly parallelized by multiplexing and with a lower setup effort, for example by using planar electrode structures in a sandwich design. Furthermore, as an electronic measuring method, automation of data processing is possible. This makes this method particularly suitable for screening systems. As a non-contact and non-invasive tool that is also used in the measurement of sensitive biological cell material,[29] polymer films can be examined directly without modification.

3. Experimental Section

Expression and Purification of the polyester hydrolases PHL7 and LCC: A detailed method is described elsewhere.[24] In short, PHL7 and LCC were recombinantly expressed as mature fusion proteins with a C-terminal His tag in *E. coli* BL21(DE3) using the pET26b(+) vector system. The intracellular fraction was purified by IMAC chromatography. The eluate obtained was treated

for 30 min at 60°C, followed by size exclusion chromatography to obtain highly purified enzyme preparations.

Manufacturing of PP/PET-Inserts: Polypropylen (PP) inserts were 3D printed one by one using an Ultimaker 3 Extended (Ultimaker BV, Netherlands) and transparent polypropylene filament (Ultimaker BV, Netherlands) at a layer resolution of 100 µm (Printing PP-inserts in parallel was not suitable, due to small defects that probably occurred because of the movement of the print head between single units). The PP surface surrounding the reaction window was roughened with emery paper. PP inserts were washed with 70 % ethanol, ultrapure water and dried at room temperature. Amorphous PET film (G-PET, thickness 250 µm ± 20 %) was purchased from Goodfellow GmbH (Bad Nauheim, Germany) and post-consumer PET thermoform clamshell packing (Guillin, Ornans, France) was obtained from a local supermarket. The PET films were cut into pieces to a size jutting out the reaction window by 2 mm to each side. PET pieces were bonded to the PP insert using epoxy resin (EPOTEK 302-3M) and fixed with two clips during curing. In order to generate a defined PET window on the outer surface, overlaying the PET film was sealed with epoxy resin.

Impedimetric Monitoring of PP/PET-Inserts: PP/PET-Inserts were cleaned for 10 min in 0.5 % SDS on a shaker, washed with ultrapure water, rinsed with 70 % ethanol and dried. Inserts were filled with 300 µL reaction buffer (1 M potassium hydrogen phosphate buffer, pH 7.8, 13.9 $\mu g \cdot mL^{-1}$ PHL7 or LCC, unless stated otherwise) and placed in a 2 mL reaction tube containing 600 µL buffer. This unit was transferred into a thermomixer (Eppendorf, Germany), closed with the electrode lid, so that one platinum electrode was placed on the inside and the other one on the outside of the PP/PET-insert. The thermomixer was set to 70°C. Platinum electrodes were connected to an in-house multiplexer controlled by a self-developed software (IMATadvanced v2021) [29b] written in LabView (National Instruments, USA). Impedance was

measured from 50 Hz to 5 MHz (61 frequency points) with a signal amplitude of 100 mV every minute with up to 6 samples in parallel using an Agilent 4294A high precision impedance analyzer (Agilent Technologies). For high-speed measurements, impedance was measured from 500 Hz to 1 MHz (35 frequency points) in a uniformly circulating multiplexing of 6 parallel samples using a Sciospec ISX-3v2 high precision impedance analyser (Sciospec GmbH) with optimized acquisition speed in the lower frequency range, thus resulting in a cycle acquisition rate of 1.3 to 1.7 s corresponding to around 250 ms per single spectrum.

Analysis of impedance data: Raw data were analyzed using the simplified *Randles* equivalent circuit model consisting of an ohmic resistor (R1) in series with the parallel combination of a capacitance (C) and a second ohmic resistor (R2). Fitting procedure was performed using a MATLAB script with the Nelder-Mead method as described elsewhere.[30] The resistance R1 corresponded to the PET-free cell resistance of the system and was derived from an impedance measurement of a PP-insert with an open reaction window using an equivalent circuit model consisting of a capacitance (C_{dl}) in series to R1. The determined R1 value (90 Ω) was used as a constant for the raw data fitting when a PET film was present, so that only C and R2 were allowed to change. Capacitance was correlated to the PET thickness assuming every change in C is caused by the thinning of the PET film (Figure S5).

Finite element model (FEM) simulation: FEM simulation was done as a 3D model using the electrical currents (ec) physics from the AC/DC-module of COMSOL Multiphysics 5.3 (Comsol Multiphysics GmbH) and a frequency domain study. Geometry data for the PET films was used from Figure S1 (4.3 x 9.1 mm^2), with buffer domains on both sides (relative permittivity: 80, electrical conductivity 11 $S \cdot m^{-1}$ measured with 1 M potassium hydrogen phosphate buffer and platinum electrode domains. For recapitulating the electrode-electrolyte double-layer, a capacitance of 0.34 $F \cdot m^{-2}$ was determined from system impedance data (Figure S2).

Additionally, the residual capacity of the whole measurement system including the measurement chamber (see Figure S4) was determined for each analyzed and simulated experiment with values in the range of 8-11 pF. This was included in the FEM model as a parallel circuit by the use of a coupled electrical circuits (cir) physics. For simulating the impedance measurement, an alternating electrical field with 100 mV amplitude at the measurement electrode and a ground connection at the counter electrode was applied. The simulation was done using a fully coupled direct solver with the mesh size normal for buffer and electrode domains, a mesh refinement step (factor 1) for the PET film domain, and a further mesh refinement step (factor 2) for the pore domain.

Optical and mechanical determination of PET film thickness

Microscopic determination of the PET film thickness was performed using PP inserts with an additional glass window on the backside to allow transmitted light images in a phase-contrast microscope (Eclipse TE2000-U, Nikon instruments Europe, BV Netherlands) with a 20 x objective lens. Inserts were placed on a microscope slide with a drop of 0.2 M potassium hydrogen phosphate buffer, pH 7.8. Top and bottom side of the PET film was focussed and the path difference was recorded using the adjustment wheel with a micrometer scaling. Thickness was then calculated according to McLaren et al. [23] using a refractive index of 1.61 for PET. Mechanical determination was performed using a digital micrometer (QuantuMike IP65, Mitutoyo).

Statistics: Graphpad Prism 5 (GraphPad Software, Inc., USA) was used for all statistical analysis. Presented graphs are given as mean ± sd unless stated otherwise. Significance of

mean difference was analyzed by one-way ANOVA and Bonferroni post-hoc test, considering *, $P < 0.05$ as significant, **, $P < 0.01$ very significant and ***, $P < 0.001$ extremely significant.

Acknowledgements

This work was funded by the Federal Ministry for Economic Affairs and Energy based on a resolution of the German Bundestag (BMWi, STARK program), the European Union (EFRE) and is co-financed from tax revenues on the basis of the budget passed by the Saxon state parliament (SMWK) (project Akto-TronikSen Grant No 100376525, Grant No 100549990).

Conflict of Interest

The authors declare no conflict of interest.

References

1. PlasticsEurope, Plastics - the Facts 2019. Brussels, 2019.
2. Bioplastics, E., What Area Bioplastics? Material Types, Terminology, and Labels: an Introduction. European Bioplastics: Berlin, 2016.
3. (a) Zhao, X.; Cornish, K.; Vodovotz, Y., Narrowing the Gap for Bioplastic Use in Food Packaging: An Update. *Environmental science & technology* **2020,** *54* (8), 4712-4732; (b) Rujnic-Sokele, M.; Pilipovic, A., Challenges and opportunities of biodegradable plastics: A mini review. *Waste management & research : the journal of the International Solid Wastes and Public Cleansing Association, ISWA* **2017,** *35* (2), 132-140.
4. Farah, S.; Anderson, D. G.; Langer, R., Physical and mechanical properties of PLA, and their functions in widespread applications - A comprehensive review. *Advanced drug delivery reviews* **2016,** *107*, 367-392.
5. Jariyasakoolroj, P.; Leelaphiwat, P.; Harnkarnsujarit, N., Advances in research and development of bioplastic for food packaging. *Journal of the science of food and agriculture* **2020,** *100* (14), 5032-5045.
6. (a) Albuquerque, P. B. S.; Malafaia, C. B., Perspectives on the production, structural characteristics and potential applications of bioplastics derived from polyhydroxyalkanoates. *International journal of biological macromolecules* **2018,** *107* (Pt A), 615-625; (b) Wang, Y.; Chen, R.; Cai, J.; Liu, Z.; Zheng, Y.; Wang, H.; Li, Q.; He, N., Biosynthesis and Thermal Properties of PHBV Produced from Levulinic Acid by Ralstonia eutropha. *PLOS ONE* **2013,** *8* (4), e60318.

7. Lee, A.; Liew, M. S., Tertiary recycling of plastics waste: an analysis of feedstock, chemical and biological degradation methods. *Journal of Material Cycles and Waste Management* **2021,** *23* (1), 32-43.
8. Kawai, F., The Current State of Research on PET Hydrolyzing Enzymes Available for Biorecycling. *Catalysts* **2021,** *11* (2), 206.
9. (a) Thiounn, T.; Smith, R. C., Advances and approaches for chemical recycling of plastic waste. *Journal of Polymer Science* **2020,** *58* (10), 1347-1364; (b) Garcia, J. M.; Robertson, M. L., The future of plastics recycling. *Science* **2017,** *358* (6365), 870-872.
10. (a) Furukawa, M.; Kawakami, N.; Tomizawa, A.; Miyamoto, K., Efficient Degradation of Poly(ethylene terephthalate) with Thermobifida fusca Cutinase Exhibiting Improved Catalytic Activity Generated using Mutagenesis and Additive-based Approaches. *Scientific reports* **2019,** *9* (1), 16038; (b) Chen, C.-C.; Dai, L.; Ma, L.; Guo, R.-T., Enzymatic degradation of plant biomass and synthetic polymers. *Nature Reviews Chemistry* **2020,** *4* (3), 114-126.
11. Kawai, F.; Kawabata, T.; Oda, M., Current knowledge on enzymatic PET degradation and its possible application to waste stream management and other fields. *Applied microbiology and biotechnology* **2019,** *103* (11), 4253–4268.
12. Chen, S.; Su, L.; Chen, J.; Wu, J., Cutinase: characteristics, preparation, and application. *Biotechnology advances* **2013,** *31* (8), 1754-67.
13. (a) Castro, A. M. d.; Carniel, A.; Stahelin, D.; Chinelatto Junior, L. S.; Honorato, H. d. A.; de Menezes, S. M. C., High-fold improvement of assorted post-consumer poly(ethylene terephthalate) (PET) packages hydrolysis using Humicola insolens cutinase as a single biocatalyst. *Process Biochemistry* **2019,** *81*, 85-91; (b) Barth, M.; Oeser, T.; Wei, R.; Then, J.; Schmidt, J.; Zimmermann, W., Effect of hydrolysis products on the enzymatic degradation of polyethylene terephthalate nanoparticles by a polyester hydrolase from Thermobifida fusca. *Biochemical Engineering Journal* **2015,** *93*, 222-228.
14. Ronkvist, Å. M.; Xie, W.; Lu, W.; Gross, R. A., Cutinase-Catalyzed Hydrolysis of Poly(ethylene terephthalate). *Macromolecules* **2009,** *42* (14), 5128–5138.
15. (a) Zhong-Johnson, E. Z. L.; Voigt, C. A.; Sinskey, A. J., An absorbance method for analysis of enzymatic degradation kinetics of poly(ethylene terephthalate) films. *Sci Rep* **2021,** *11* (1), 928; (b) Belisario-Ferrari, M. R.; Wei, R.; Schneider, T.; Honak, A.; Zimmermann, W., Fast Turbidimetric Assay for Analyzing the Enzymatic Hydrolysis of Polyethylene Terephthalate Model Substrates. *Biotechnology journal* **2019,** *14* (4), e1800272.
16. Pirillo, V.; Pollegioni, L.; Molla, G., Analytical methods for the investigation of enzyme-catalyzed degradation of polyethylene terephthalate. *The FEBS journal* **2021**.
17. Syedd-León, R.; Sandoval-Barrantes, M.; Trimiño-Vásquez, H.; Villegas-Peñaranda, L. R.; Rodríguez-Rodríguez, G., Revisiting the fundamentals of p-nitrophenol analysis for its application in the quantification of lipases activity. A graphical update. *Uniciencia* **2020,** *34* (2), 31-43.

18. (a) Ana, G. R.-H.; Muñoz-Tabares, J. A.; Aguilar-Guzmán, J. C.; Rafael, V.-D., A novel and simple method for polyethylene terephthalate (PET) nanoparticle production. *Environmental Science: Nano* **2019,** *6* (7), 2031-2036; (b) Vogel, K.; Wei, R.; Pfaff, L.; Breite, D.; Al-Fathi, H.; Ortmann, C.; Estrela-Lopis, I.; Venus, T.; Schulze, A.; Harms, H.; Bornscheuer, U. T.; Maskow, T., Enzymatic degradation of polyethylene terephthalate nanoplastics analyzed in real time by isothermal titration calorimetry. *The Science of the total environment* **2021,** *773*, 145111.
19. Sabot, A.; Krause, S., Simultaneous Quartz Crystal Microbalance Impedance and Electrochemical Impedance Measurements. Investigation into the Degradation of Thin Polymer Films. *Analytical Chemistry* **2002,** *74* (14), 3304-3311.

20. Fernández-Sánchez, C.; McNeil, C. J.; Rawson, K., Electrochemical impedance spectroscopy studies of polymer degradation: application to biosensor development. *TrAC Trends in Analytical Chemistry* **2005,** *24* (1), 37-48.
21. (a) Randles, J. E. B., Kinetics of rapid electrode reactions. *Discussions of the Faraday Society* **1947,** *1*, 11; (b) Ahmed, R.; Reifsnider, K., Study of Influence of Electrode Geometry on Impedance Spectroscopy. 2010; pp 167-175.
22. Küchler, F.; Färber, R.; Franck, C. M. In *Humidity and Temperature Effects on the Dielectric Properties of PET Film*, 2020 IEEE Electrical Insulation Conference (EIC), 22 June-3 July 2020; 2020; pp 179-183.
23. McLaren, J. W.; Nau, C. B.; Erie, J. C.; Bourne, W. M., Corneal thickness measurement by confocal microscopy, ultrasound, and scanning slit methods. *American journal of ophthalmology* **2004,** *137* (6), 1011-20.
24. Sonnendecker, C.; Oeser, J.; Richter, P. K.; Hille, P.; Zhao, Z.; Fischer, C.; Lippold, H.; Blazquez-Sanchez, P.; Engelberger, F.; Ramirez-Sarmiento, C. A.; Oeser, T.; Lihanova, Y.; Frank, R.; Jahnke, H. G.; Billig, S.; Abel, B.; Strater, N.; Matysik, J.; Zimmermann, W., Low Carbon Footprint Recycling of Post-Consumer PET Plastic with a Metagenomic Polyester Hydrolase. *ChemSusChem* **2021,** *n/a* (n/a).
25. Zhao, Y. P.; Wang, G. C.; Lu, T. M.; Palasantzas, G.; De Hosson, J. T. M., Surface-roughness effect on capacitance and leakage current of an insulating film. *Physical Review B* **1999,** *60* (12), 9157-9164.
26. (a) Sulaiman, S.; Yamato, S.; Kanaya, E.; Kim, J. J.; Koga, Y.; Takano, K.; Kanaya, S., Isolation of a novel cutinase homolog with polyethylene terephthalate-degrading activity from leaf-branch compost by using a metagenomic approach. *Applied and environmental microbiology* **2012,** *78* (5), 1556-62; (b) Sulaiman, S.; You, D. J.; Kanaya, E.; Koga, Y.; Kanaya, S., Crystal structure and thermodynamic and kinetic stability of metagenome-derived LC-cutinase. *Biochemistry* **2014,** *53* (11), 1858-69.
27. Liu, B.; Lu, X.; Ju, Z.; Sun, P.; Xin, J.; Yao, X.; Zhou, Q.; Zhang, S., Ultrafast Homogeneous Glycolysis of Waste Polyethylene Terephthalate via a Dissolution-Degradation Strategy. *Industrial & Engineering Chemistry Research* **2018,** *57* (48), 16239-16245.
28. Wang, S.; Meng, X.; Zhou, H.; Liu, Y.; Secundo, F.; Liu, Y., Enzyme Stability and Activity in Non-Aqueous Reaction Systems: A Mini Review. *Catalysts* **2016,** *6* (2).
29. (a) Eichler, M.; Jahnke, H. G.; Krinke, D.; Muller, A.; Schmidt, S.; Azendorf, R.; Robitzki, A. A., A novel 96-well multielectrode array based impedimetric monitoring platform for comparative drug efficacy analysis on 2D and 3D brain tumor cultures. *Biosensors & bioelectronics* **2015,** *67*, 582-9; (b) Jahnke, H. G.; Krinke, D.; Seidel, D.; Lilienthal, K.; Schmidt, S.; Azendorf, R.; Fischer, M.; Mack, T.; Striggow, F.; Althaus, H.; Schober, A.; Robitzki, A. A., A novel 384-multiwell microelectrode array for the impedimetric monitoring of Tau protein induced neurodegenerative processes. *Biosensors & bioelectronics* **2017,** *88*, 78-84.
30. Steude, A.; Schmidt, S.; Robitzki, A. A.; Panke, O., An electrode array for electrochemical immuno-sensing using the example of impedimetric tenascin C detection. *Lab on a chip* **2011,** *11* (17), 2884-92.

TABLE OF CONTENTS

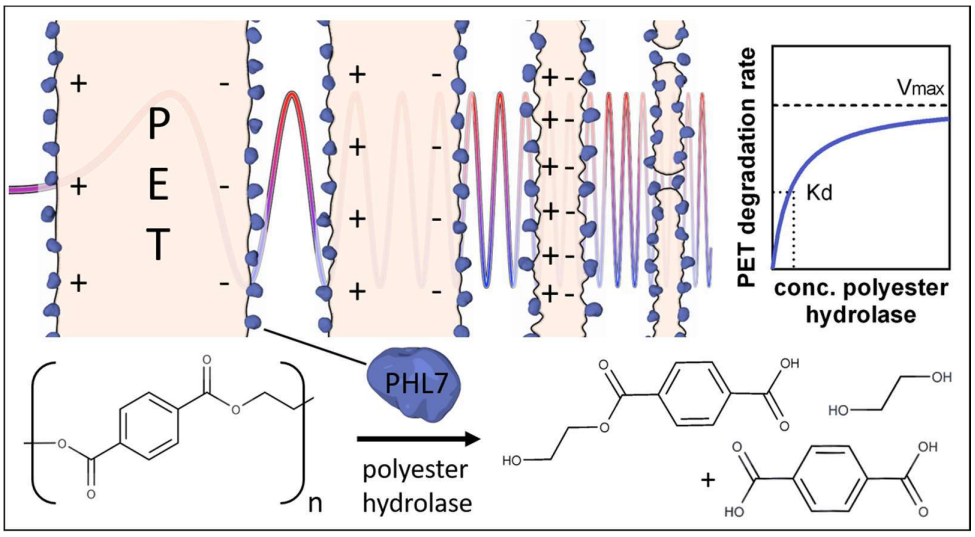

Enzymatic recycling of post-consumer PET provides a sustainable solution for the recovery of polymer precursors. This study demonstrates how to benchmark enzyme performance based on the dielectric properties of PET films in a multiplexed electronic measurement. The method features real-time data acquisition, scalability, and robustness to additives to accelerate the search for PET- and for plastic-degrading biocatalysts, in general.